An Orphan stream, dark matter subhalos and the missing satellites in the Aquarius simulations.

Joren Heit
Supervisor: Amina Helmi

August 3, 2012

Contents

1 Introduction

One of the major open issues in modern astrophysics concerns the large amounts of matter that are invisible to not only the naked eye, but also to all of our instruments. It is a kind of matter that only seems to interact with the familiar matter through gravity, which is how we know it must be there. Observations throughout the previous century have shown that the dynamics of stars in galaxies (the rotation curves, for example) imply the presence of amounts of matter that exceed what can be accounted for by the visible matter. It is estimated that 85% percent of all matter must be Dark Matter (DM). Although the DM may explain the internal dynamics of galaxies, it has been postulated that on an even larger scale it is Dark Energy (DE) that is ruling the history and fate of the Universe. In the context of the project described here, however, DE is only considered to affect the cosmological model in which our study is embedded.

Galaxies are surrounded by dark matter halos and even for our own Milky Way (MW) galaxy, little is known about about its mass distribution. Cosmological N-body simulations involving very large numbers of particles, have shown that a MW-like galaxy is very likely to have a DM-halo with substantial substructure [1][1] . This means that within this smooth halo, smaller satellites, or subhalos, are orbiting, yielding a 'lumpy' gravitational potential. One might expect star-formation to take place in dense parts of a DM-clump and be observable within the MW or the nearby Andromeda Galaxy (M31). However, the number of DM-satellites predicted by simulations is significantly largely than the number of observed satellites of both the MW and M31 [2]. This probably means that –even after taking into account the possibility that we are just overlooking these satellites– there must also be dark satellites, or dark subhalos out there.

One of the few ways of measuring, or constraining the shape and mass distribution of dark matter halos is by looking at tidal streams that orbit in the stellar halos of galaxies. A stellar stream, such as that shown in Figure 1, is a (relatively small) group of stars that originate in a dwarf galaxy or globular cluster. Because of the host galaxy's tidal force[2] that acts on this small system, it gradually loses stars that will follow roughly the same orbit, either trailing behind or leading the parent object. In a smooth potential, the result is a cold and thin stream that nearly traces a single orbit. This means that any perturbations in the gravitational potential should become apparent. By observing stars in the sky that are part of the same stream, we can map part of the orbit that this stream is following, and this yields information about the potential (mass distribution) of the host halo.

This being said, the problem discussed in this report can be formulated. A recent set of numerical simulations –the most vast up until now– has shed new light on the evolution of DM-(sub)structure within a MW-like halo. This suite of simulations constitutes the Aquarius Project which was completed in 2008. The focus of this report will be on a particular stream formed in one of the Aquarius halo's (Aq-A-2) (Figure 1), reported in Helmi et al. [3]. At present day ($z = 0$), this stream showed a granular appearance unlike that expected in a smooth potential. In a smooth halo, a stream will have a relatively continuous density and will become wider and elongated along its orbit in time, depending for example on the shape of the potential. Therefore, the question is what is the cause of the lumpy and perturbed appearance of this stream. A potential cause of these observations could be the occurrance of multiple collisions between the satellite stream and dark subhalos. This project will focus on the detection of such collisions to determine how frequently they occur and if their consequences can be measured.

Johnston et al. [4] studied the effects on clumpy potentials on thin streams. They found that it should be possible to distinguish between a smooth or lumpy Milky-Way halo by quantifying the coldness of the stream. One of the features of a stream that orbits in a lumpy potential, is a very irregular radial velocity distribution. Ibata et al. [5] found that, even in a nearly spherical potential, the remnants of a globular cluster will become substantially dispersed over the sky when subhalos are included. Also, they find that the presence of substructure leads to a large dispersion

[1]It is estimated that 10-20% of the total mass is in the substructure of a dark halo. This still means that the vast majority is in the smooth part of the halo.

[2]Tidal forces are the result of the gravitational force on a body (a dwarf galaxy in this case), which is not constant accross the diameter of the object. The stars in the satellite galaxy that are nearest to the host centre, where the density is highest, experience a slightly greater force than the stars on the other side. This will eventually result in a deformation of the satellite galaxy and the gradual loss of mass.

in the angular momentum, in particular the z component L_z. Yoon et al. [6] found that the distribution of angular momentum versus energy should incorporate visible gaps. This was not noticed by Ibata et al., but in retrospect these gaps, albeit much less obvious, were also present in their simulations. These previous works ([4], [5], [6]) have all been set up in more or less idealized conditions. We will investigate if similar features exist in the Aquarius simulations, which are more realistic and complex beacause they are fully cosmological.

Figure 1: Two streams in galactic coordinates identified in the Aquarius simulations by Helmi et al. [3]. The discontinuities in the density of this suggest it may have been perturbed during its lifetime.

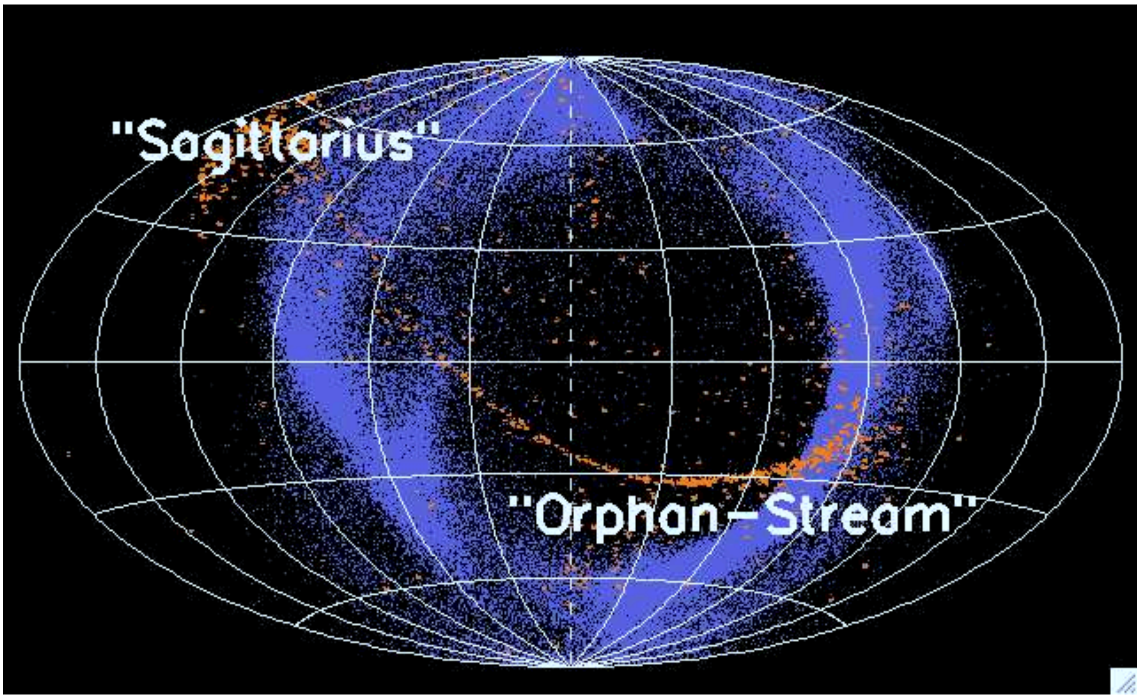

2 The Aquarius Project

As mentioned in the Introduction, this research will be based on the outputs of the Aquarius Project. Below we present a short summary of the characteristics of the simulations and how they were set up.

2.1 Simulations

Within a periodic cubic box with side $100\,\mathrm{h}^{-1}$ Mpc $\simeq$ 137 Mpc, a total number of 900^3 particles was placed using initial conditions as explained in Section 2.1 of [1]. With gravity being the only force present, the time evolution of these particles was followed for ~ 13.7 Gyr (the approximate age of the Universe) during which the large-scale cosmic web developed and massive dark matter halos were formed. From this low resolution simulation, a number of Milky-Way-like halos were selected, having roughly the same mass and without any large close neighbours. These halos were re-simulated using a so-called 'zoom-in technique' (Figure 2), where the halo volume was split up in two regions: a high-resolution and a low-resolution region. Within the high-resolution region, the mass distribution was represented by a much larger number of particles of lower mass than the original ones. More distant regions were filled with increasingly more massive particles (as opposed to the high-resolution volume, in which all particles have the same mass), yielding a lower resolution volume, but still large enough to ensure an accurate representation of the tidal field. The resimulations were carried out at a maximum of 5 different resolutions (resolution 1 representing the highest number of particles), for 6 different (main) halo's (A-F) and then coded Aq-[A-F]-[1-5]. Since this report mainly uses results from the Aq-A-2 halo, we list the properties of different resolutions of the Aq-A halo in Table 1.

Figure 2: The left picture displays the result of the large volume, low resolution simulation (box is 137 Mpc). From this present-day output, six different Milky Way-like halo's were selected to be re-simulated with the zoom-in technique. The right picture shows the result of this resimulation for Aq-A-2.

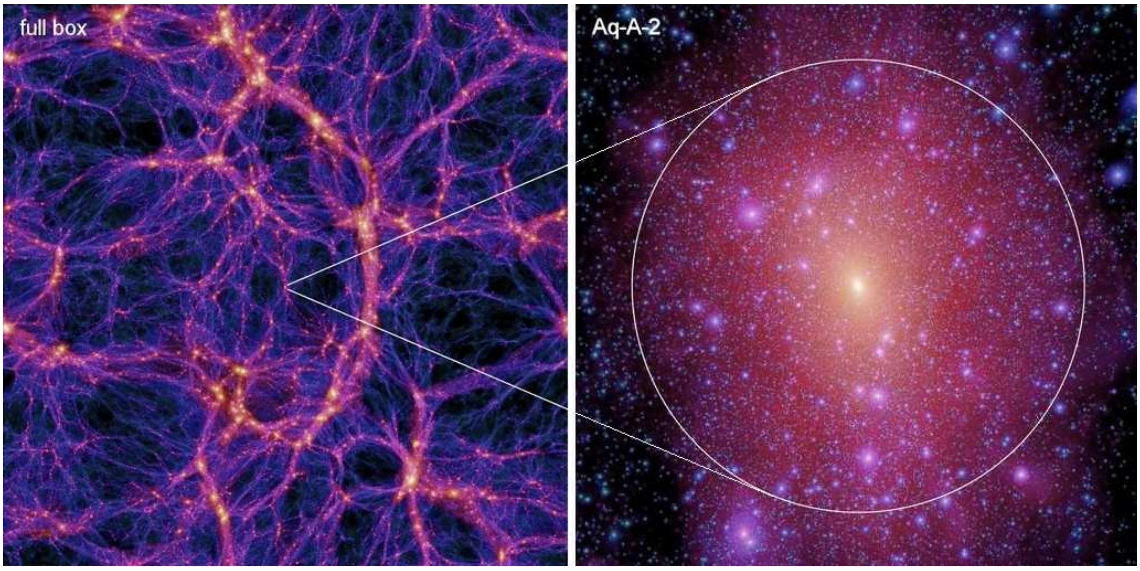

Table 1: Some properties of the Aq-A halos. Listed below are the properties of the five different resolution runs where m_p is the particle mass, N_{hr} is the number of high-resolution particles and N_{lr} is the number of low resolution particles.

Name	$m_p(M_\odot)$	N_{hr}	N_{lr}
Aq-A-1	1.172×10^3	4252670000	144979154
Aq-A-2	1.370×10^4	531570000	75296170
Aq-A-3	4.911×10^4	148258000	20035279
Aq-A-4	3.929×10^5	18535972	634793
Aq-A-5	3.143×10^6	2316893	634793

The re-simulated halos depict a large amount of substructure, or DM-subhalos, as is visible in the right panel of Figure 2 and was described by Springel et al. (2008) [1]. The SUBFIND algorithm has been run on these simulations to identify subhalos a locally overdense structures containing at least 20 bound particles. A total of 113,284 subhalo's could be identified in Aq-A-2 at $z = 0$ and their abundance by mass is plotted in Figure 3, in which can be seen that it has a power law with exponent -0.83:

$$N(m > M) \propto M^{-0.83} \tag{1}$$

For the Aq-A-2 halo there are 128 snapshots (Table 2), starting from redshift ~ 46 up to the present day. For each of these snapshots, all subhalos were found and the position/velocity vectors of the most-bound particles were recorded. These particles are tagged with a unique identification number ID_{MB}. The number of particles bound to the subhalo can be used to estimate the total mass of the object (Table 1).

Because these most-bound particles are independently identified, it is possible that the same subhalo has a different ID_{MB} at different snapshots. Therefore, subhalos from different (subsequent) snapshots may be linked as being the descendant of a given subhalo identified earlier. This can be due to the fact that it accreted or merged with another subhalo, or simply because another particle accidentally became most-bound. Therefore, to trace a subhalo in time, the ID's of the 20

Figure 3: Subhalo abundance by mass. The relation is clearly a power-law: $N(m > M) \propto M^{-0.83}$.

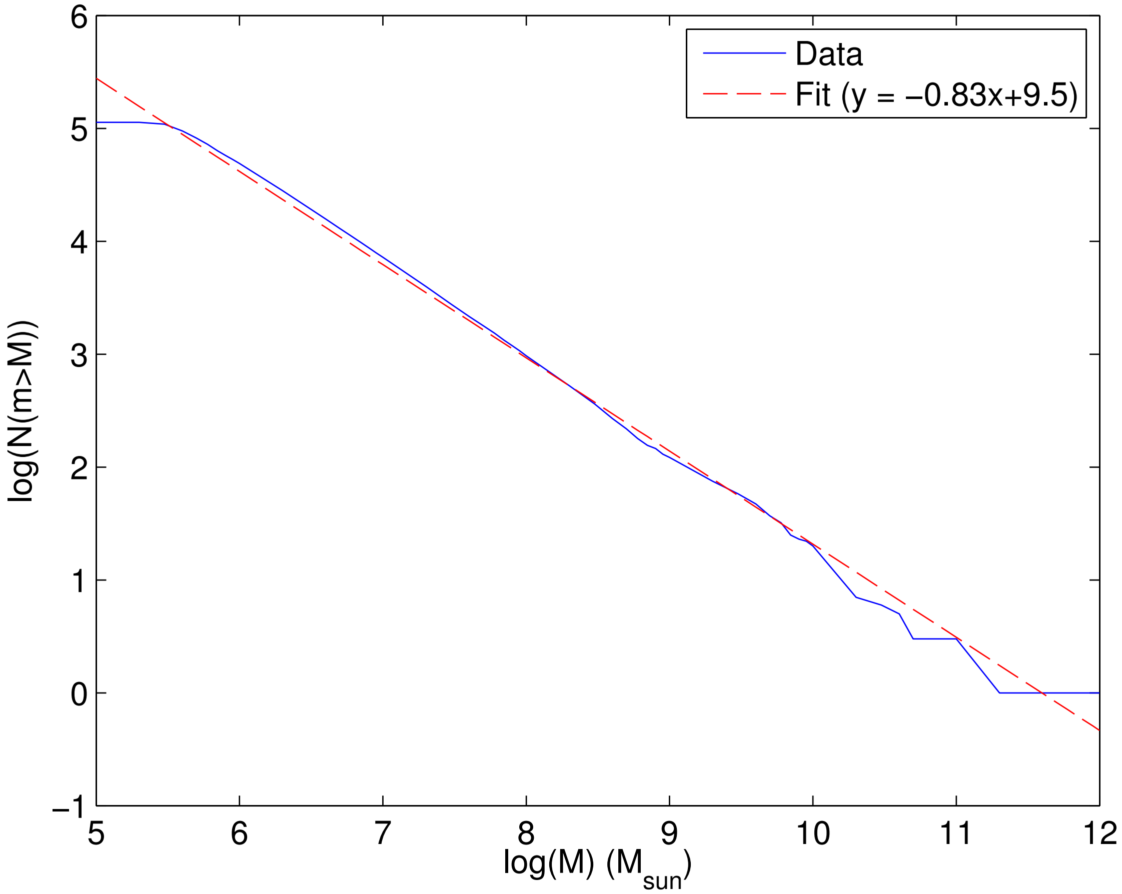

per cent most bound particles at each snapshot are recorded and compared between subsequent snapshots to identify the subhalo's descendant or progenitor.

2.2 Generating the stellar component

The halos in the Aquarius simulations consist of DM particles only, i.e. they do not contain a baryonic (stellar of gaseous) component. Nonetheless, using these simulations in combination with semi-analytic models of galaxy formation, it is possible to follow, for example, the formation of a stellar halo. Cooper et al (2010) [7] tagged a subset of all DM particles as 'stars', or actually stellar populations. Moreover, from now we will simply refer to the tagged DM particles as stars. The particles were tagged under the assumption that the most-bound DM particles would have similar dynamics as the stars, as these are found in the deepest part of the potential wells of dark halos. Thus, particles within the halo are sorted by binding-energy and at each snapshot, a most-bound fraction f_{MB} is chosen to be tagged with newly formed stars as given by the semi-analytical model, resulting in a growing stellar population over time. The value of the parameter f_{MB} was determined by comparing the structure and kinematics of the resulting luminous satellites at $z = 0$ to Local Group dwarf galaxies. It turned out that $f_{MB} = 1\%$ gave the best results. Simply tagging DM particles like this is a major simplification, but Cooper et al. have shown that this method resulted in realistic stellar halos, both in terms of assembly and structure. In this report, this coupling between the available stellar and DM data will be assumed. The most bound DM particle (identified by SUBFIND) is used to trace the location and dynamics of the center of mass of the satellite galaxy until it is fully disrupted. Moreover, from now we will simply refer to the tagged

Table 2: Relation between the 128 available outputs of the Aq-A-2 halo and redshift/age of the Universe. Note that the time-intervals are non-constant.

output	z	t (Gyr)	output	z	t (Gyr)	output	z	t (Gyr)
1	46.7554	0.054117	51	3.7083	1.7399	101	0.40136	9.406
2	44.596	0.058007	52	3.4933	1.8649	102	0.3822	9.5605
3	42.5342	0.062176	53	3.2878	1.9989	103	0.36347	9.7151
4	40.5657	0.066645	54	3.0914	2.1426	104	0.34517	9.8697
5	38.6861	0.071435	55	2.9048	2.2956	105	0.32728	10.0243
6	36.8916	0.076569	56	2.736	2.4501	106	0.30978	10.1788
7	35.1782	0.082072	57	2.5837	2.6047	107	0.29265	10.3334
8	33.5422	0.087971	58	2.4456	2.7593	108	0.27589	10.488
9	31.9803	0.094294	59	2.3197	2.9138	109	0.25947	10.6426
10	30.4889	0.10107	60	2.2041	3.0684	110	0.24339	10.7971
11	29.065	0.10834	61	2.0977	3.223	111	0.22763	10.9517
12	27.7055	0.11612	62	1.9993	3.3776	112	0.21219	11.1063
13	26.4074	0.12447	63	1.9079	3.5321	113	0.19704	11.2609
14	25.1681	0.13341	64	1.8228	3.6867	114	0.18219	11.4154
15	23.9847	0.143	65	1.7432	3.8413	115	0.16762	11.57
16	22.8549	0.15328	66	1.6687	3.9959	116	0.15331	11.7246
17	21.7761	0.1643	67	1.5986	4.1504	117	0.13927	11.8792
18	20.7462	0.17611	68	1.5326	4.305	118	0.12549	12.0337
19	19.7627	0.18876	69	1.4703	4.4596	119	0.11195	12.1883
20	18.8238	0.20233	70	1.4113	4.6142	120	0.098645	12.3429
21	17.9273	0.21687	71	1.3554	4.7687	121	0.085574	12.4975
22	17.0713	0.23246	72	1.3023	4.9233	122	0.072728	12.652
23	16.254	0.24917	73	1.2517	5.0779	123	0.060099	12.8066
24	15.4737	0.26708	74	1.2035	5.2325	124	0.04768	12.9612
25	14.7286	0.28627	75	1.1576	5.387	125	0.035467	13.1158
26	14.0172	0.30685	76	1.1136	5.5416	126	0.023453	13.2703
27	13.3379	0.3289	77	1.0715	5.6962	127	0.011632	13.4249
28	12.6894	0.35254	78	1.0311	5.8508	128	0	13.5795
29	12.0701	0.37788	79	0.99237	6.0053			
30	11.4788	0.40504	80	0.95514	6.1599			
31	10.9143	0.43415	81	0.91932	6.3145			
32	10.3752	0.46536	82	0.88482	6.4691			
33	9.8605	0.4988	83	0.85156	6.6236			
34	9.369	0.53466	84	0.81947	6.7782			
35	8.8997	0.57308	85	0.78847	6.9328			
36	8.4515	0.61427	86	0.7585	7.0874			
37	8.0236	0.65842	87	0.7295	7.2419			
38	7.615	0.70575	88	0.70143	7.3965			
39	7.2248	0.75647	89	0.67421	7.5511			
40	6.8522	0.81084	90	0.64782	7.7057			
41	6.4964	0.86912	91	0.62221	7.8602			
42	6.1566	0.93158	92	0.59734	8.0148			
43	5.8321	0.99854	93	0.57317	8.1694			
44	5.5221	1.0703	94	0.54966	8.3239			
45	5.2261	1.1472	95	0.52679	8.4785			
46	4.9433	1.2297	96	0.50453	8.6331			
47	4.6733	1.3181	97	0.48284	8.7877			
48	4.4153	1.4128	98	0.46171	8.9422			
49	4.1688	1.5144	99	0.44109	9.0968			
50	3.9333	1.6232	100	0.42099	9.2514			

DM particles as stars.

The stellar data is also available as a set of 128 snapshots, and contains the position and velocity vectors of all identified stars. Each star has been given a unique identification number, $ID_{stellar}$, in order to be able to trace individual stars through time. In addition, each star also contains the ID of its host system, $ID_{satellite}$, which can be used to trace all members of a specific satellite.

3 Methods

As mentioned in the Introduction, the stream in Figure 1, present in the Aq-A-2 halo, has a disturbed appearance at the current epoch. In analogy to the field of streams discovered in the SDSS by Belokurov et al. [8], this stream was named the *Orphan Stream* because of its stellar mass and location. The question that constitutes the central question of this report is: "What was the cause behind the perturbations visible in this Orphan stream?". Some of the properties of this stream are listed in Table 3.

Table 3: Properties of the Orphan stream.

Name	Orphan
Number of particles	857
Time of accretion (t_{accr})	$1.23 Gyr$
Stellar mass (M_*)	$10^5 M_\odot$
Dark Mass (M_{DM})	$1.2 \times 10^8 M_\odot$

To get an initial idea of some other properties of this Orphan stream, its evolution is plotted in Figure 4. We can see that around 5-6 Gyr the stream is starting to form, i.e. stars gradually become unbound and start trailing behind or leading the satellite. Rather than measuring the centre of mass at each snapshot, which is difficult once stars become unbound, we take the center to be the most-bound DM-particle of the subhalo which hosts the Orphan-stars (see also section 2.2). This coordinate can also be used to trace the center of the satellite in time, yielding its orbit. This orbit is plotted in 3 Cartesian projections in Figure 5. Here we see how the object is accreted by the main Aq-A-2 halo at early times. Its galactocentric distance is plotted in Figure 6.

Because the time sampling of the data is sparse after snapshot 54, ~ 2 Gyr, an interpolation between snapshots was made to smoothen the visual appearance of the orbit. Figure 6 shows a peculiar and sudden shift in amplitude to take place at around 7.5 Gyr. In a smooth time-independent potential, particles on regular orbits would oscillate at constant frequency and nearly the same amplitude. In a non-spherical potential the minimum and maximum galactocentric distances will vary, but with a regular frequency. We can clearly see non-regular variations in these orbital parameters in Figure 5. The cause of the first large radial excursions seen in Figure 5 and 6 correspond to times when this object was forming, decoupling from the expansion of the Universe and evolving independently of the final host halo. Thus from now on, we restrict our analysis to times after the object became a satellite of the main halo, i.e. from $t_{accr} \sim 1.23$ Gyr onwards[3]. The cause of the change in amplitude of the oscillations at $t \sim 7.5$ Gyr is less clear, and could be related to an interaction with a dark subhalo. However, we do not have at this point in time enough time-resolution in our snapshots to be able to test this hypothesis.

4 Collisions

In this section, the positions of the DM-subhalos orbiting the main Aquarius halo will be compared to those of the stars in the Orphan stream. We would like to quantify how common close encounters are or if every dwarf galaxy is bound to run in to one or more at some point in its evolution. Yoon et al. (2011) [6] already saw that in idealized conditions, characteristic for a Milky-Way-like halo,

[3]The time of accretion t_{accr} is actually defined as the time when the object came within the halo's virial radius r_{vir} for the first time. The virial radius is defined as the radius that encloses a sphere of a mean density that is 200 times (by convention) the critical density of the Universe.

Figure 4: Series of 16 snapshots starting at $z = 1.8$, showing the formation and evolution of the stream into a rather perturbed structure. The plots are centered on the most-bound DM-particle of the object (in the XY-plane). Each tick-mark is equal to 50 kpc, i.e. the boxes are square and 200 kpc on a side.

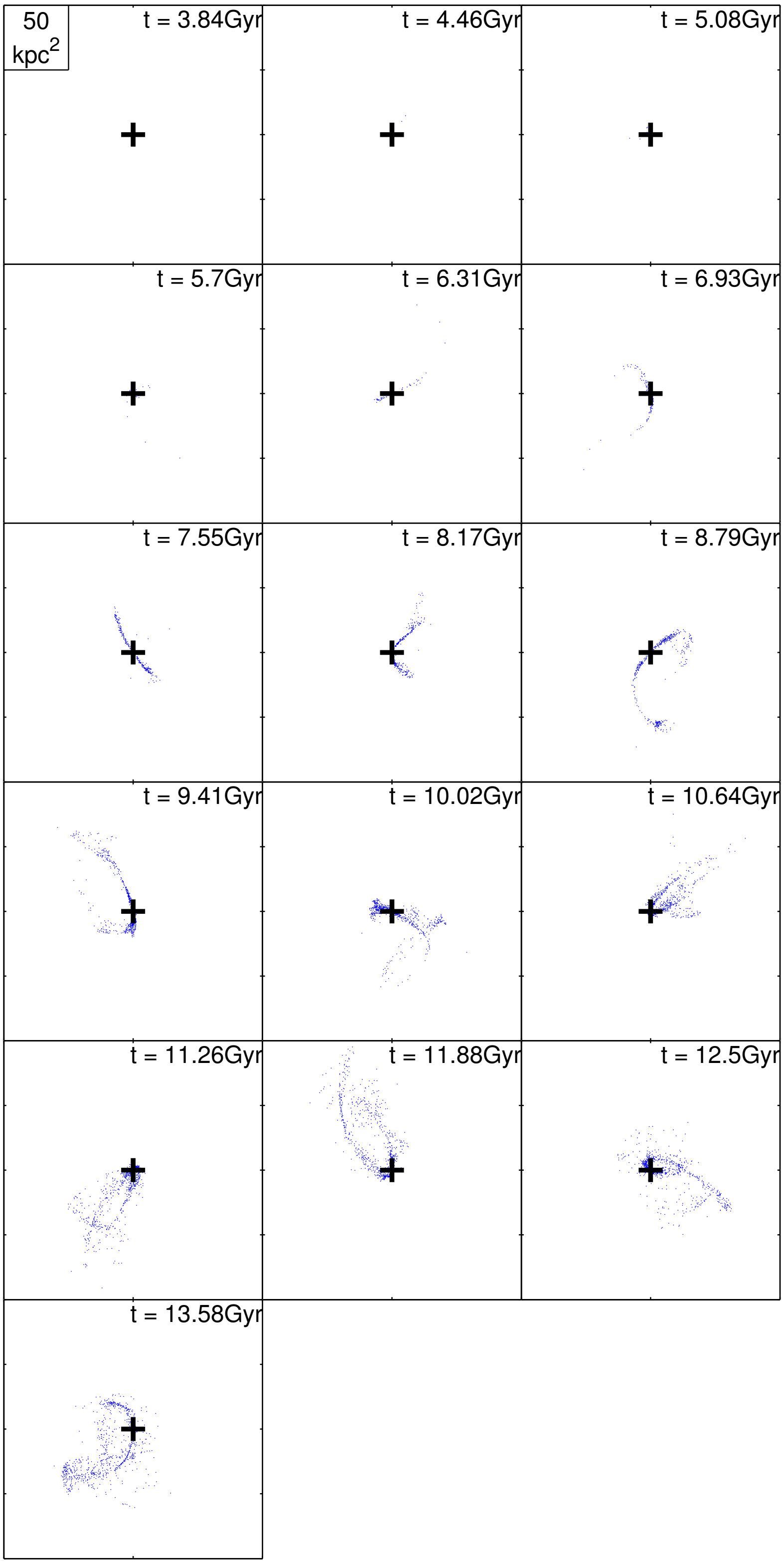

Figure 5: The orbit of the satellite's most-bound particle in the XY,XZ and YZ planes respectively. The time-span is the same as that of Figure 6 (13.7 Gyr)

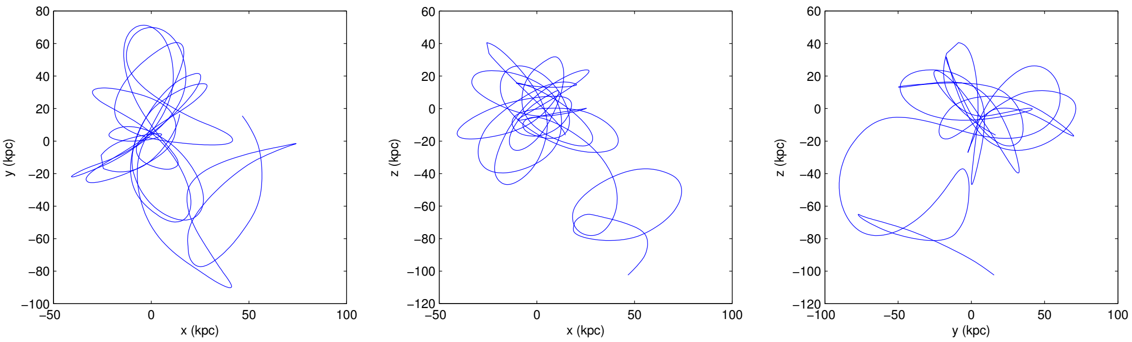

Figure 6: Distance between the satellite and the centre of the main Aquarius halo. The time of accretion is defined as the time when this object first came within the virial radius r_{vir} of this halo.

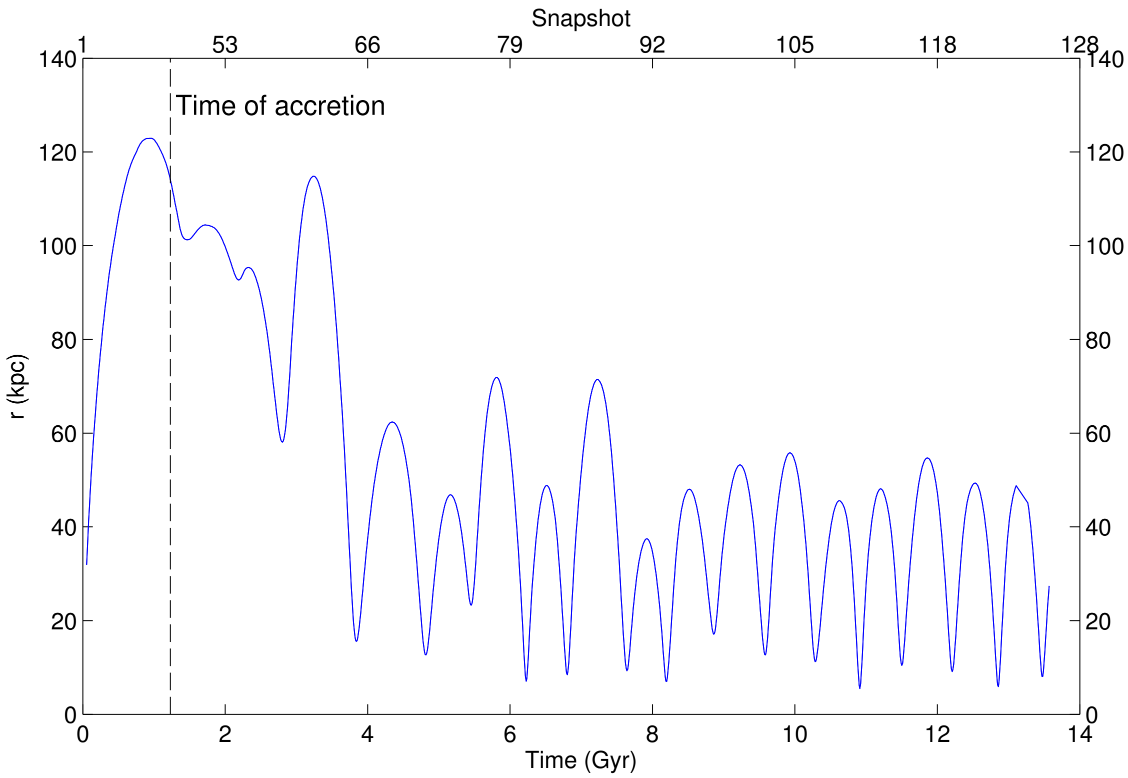

a simulated stream similar to Palomar 5 (Pal 5) suffers hundreds of encounters with objects less massive ($\lesssim 10^5\,M_\odot$), of the order of a few tens of encounters with objects in the range $10^5 - 10^7\,M_\odot$ and even a few encounters with objects of masses between $10^7\,M_\odot$ and $10^8\,M_\odot$.

These encounters however will not completely change the velocity vectors of stars in the stream, as they are still relatively weak encounters. In contrast, a strong encounter [9] is defined as an encounter that completely changes the the speed and direction of motion of a star. Therefore, an encounter is labeled *strong* when the change in potential energy at their closest approach is at least as great as the kinetic energy of the star before the encounter.

$$\frac{GM_{star}M_{sub}}{b} \geq \frac{M_{star}v_{rel}^2}{2} \tag{2}$$

Solving for M_{sub} and setting the impact parameter $b = 2$kpc, we find that using these definitions, a strong encounter within 2 kpc would require the subhalo to be very massive: $M_{sub} \geq 2.6 \times 10^{10}\, M_\odot$. The relative speed was set to the typical relative speed v_{rel}^{typ} which can be estimated from the velocity dispersion parameter (using $v_{vir} \simeq 180$ km/s [1])

$$\sigma \simeq \frac{v_{vir}}{\sqrt{2}} \simeq 127\,\mathrm{km/s} \tag{3}$$

The typical relative velocity (Yoon et al. [6]) is therefore

$$v_{rel}^{typ} = \frac{3}{2}\sqrt{\pi}\sigma \;\approx 340\mathrm{km/s} \tag{4}$$

Objects as massive as $2.6 \times 10^{10}\, M_\odot$ *do* exist, although they are rarer, as shown in Figure 3 for the Aq-A-2 halo. The odds of strong encounters happening as described by Equation 2 are thus very small. We will now discuss how many encounters the satellite suffered during its lifetime, without making a distinction in terms of the mass of the perturber subhalo.

4.1 Counting the number of collisions

4.1.1 Collisions with the center

To measure the number of collisions, we count how often a subhalo comes within a distance of b kpc of a star. First, the number of encounters with the most-bound particle associated to the stellar stream will be counted. The position of the most-bound particle is, as discussed before, taken to be at the center, first of the satellite galaxy and later on, of the stellar stream. We denote this position with $\mathbf{r}_c$. For every snapshot, $\mathbf{r}_c$ will be calculated to find the distance d to all subhalo's. The distance from the core to the j^{th} subhalo is then given by

$$d_{c,j} = \sqrt{\sum_{i=1}^{3}(x_c^i - x_j^i)^2} \tag{5}$$

At each snapshot, this is done for all values of j, i.e. all the subhalos present, and the number of times $d_{c,j} < b$ is counted. The results for $b = 2, 5, 10$ kpc are plotted in Figure 7. This figure shows that there were no encounters within a radius of 1 kpc from the center of the stream.

The peak at early times arises because during this stage the satellite galaxy itself is still being assembled. It merges with other galaxies and halos before it finally settles as a satellite of the main Aquarius halo. Hereafter, a number of small peaks can be seen. Each peak corresponds to a close encounter with a subhalo, and we have checked that these encounters are all with different objects. This means that in the available 81 snapshots (48 - 128), i.e. after the object became a satellite and until the present day, a total number of 16 encounters are observed that occur within a distance of 2 kpc. Remember that the time sampling is not optimal, ($\Delta t = 0.1546$ Gyr/snapshot), so it is very probable that there are intermediate times at which a dark object is close to the center of the stream but we are not able to detect it. We expect this since to cross the volume of radius $b = 2$ kpc within this time-frame only requires a velocity $v_{sub}^{\perp} = \frac{2b}{0.1546\mathrm{Gyr}} \simeq 25\frac{\mathrm{km}}{\mathrm{s}}$ and the speeds of nearly all objects greatly exceed this number (Figure 10).

4.1.2 Collisions with any star

Of course, collisions between subhalos and any stream-star are also possible. This is why we also count how many encounters are observed between dark objects and each individual member of our Orphan stream. To measure this number, the distance to all subhalos was calculated for each star, and all subhalo's within b kpc of the given star were registered. Figures 8 and 9 show a graphical representation of two snapshots, including the location of the nearest dark subhalos. Figure 10

Figure 7: Number of collisions with the most-bound particle of our Orphan stream progenitor as a function of time for $b = 2, 5, 10$kpc

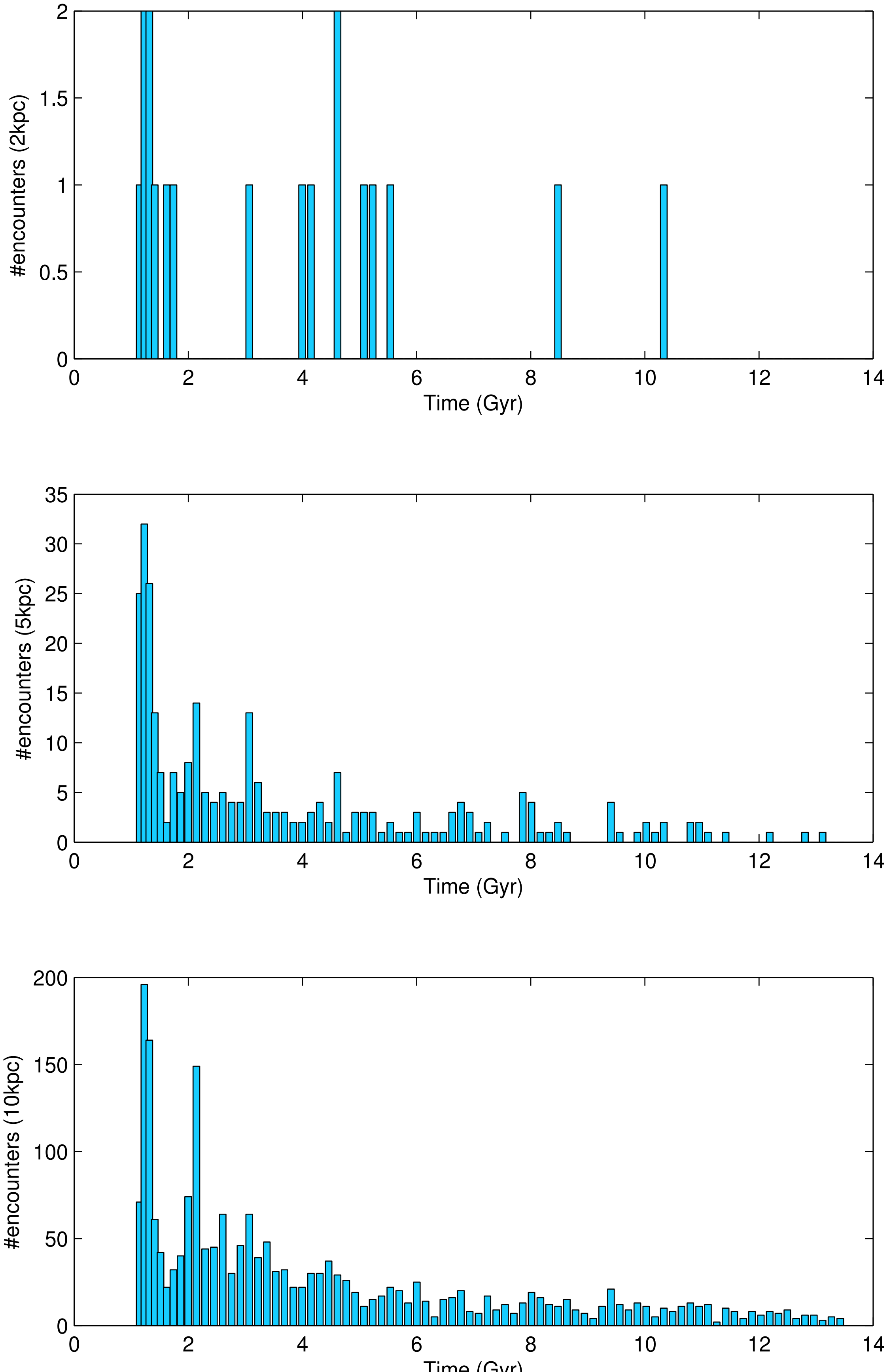

can be used to estimate the absolute velocity of the subhalos shown in Figures 8 and 9. From these figures it can be seen that many stars have an encounter with the same subhalo. Therefore, in order to count independent collisions, at each snapshot the unique set of close subhalos was determined and the number of members of this set was counted. The resulting number is heavily dependent on the impact parameter b, which can be seen from Figure 11. Another visible trend in these figures is that the number of encounters grows with time. This is most likely due to the increase in volume of the stream. As time passes, the stream is both elongated and widened, thus increasing the total volume in which encounters are registered (i.e. the cross section of encounters becomes larger). This same trend is not visible in the number of encounters with the center of mass because the volume is constant in this case, resulting in a more or less constant rate of encounters, in the range of 0-2 encounters per snapshot within a distance of 2 kpc. In both cases, it can be assumed that the subhalos that pass within 1 or 2 kpc of a star, actually overlap with the stream since they are extended, i.e. they have a finite volume extent.

Figure 8: At $t = 4$ Gyr, the stream has not formed yet and the satellite (red) is accompanied by only one dark object (black). For this particular snapshot, one encounter will be counted. The results for all snapshots are given in Figure 11. Figure (a) shows both objects with the satellite center indicated as a blue dot together with its velocity vector (color-coded according to Figure 10), where (b) shows only the dark object with its velocity vector. The vector color indicates the absolute velocity of this object, which can be estimated from Figure 10.

(a) The satellite together with the only subhalo that passes within 2kpc at t=4Gyr.

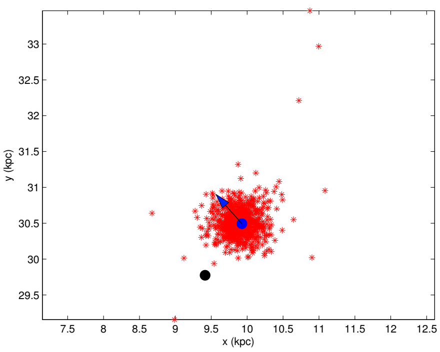

(b) The dark object from Figure (a) with its velocity vector. See also the color index in Figure 10.

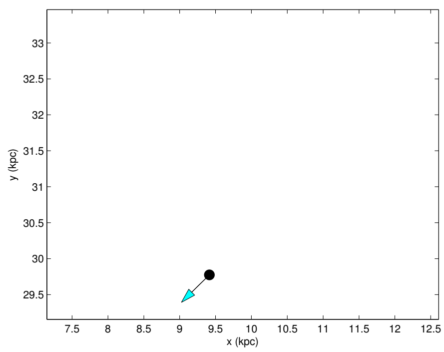

Figure 9: At $t = 10$ Gyr, the stream (red) has 19 nearby dark objects (black). The blue dot indicates the position of the satellite's most-bound particle, and the velocity vector that goes along with it is color-coded according to Figure 10. In this case, 19 encounters are registred. The results for all snapshots are given in Figure 11. The vector color indicates the absolute velocity of the objects, which can be estimated from Figure 10.

(a) The satellite together with all subhalo's that pass within 2 kpc at t=10Gyr.

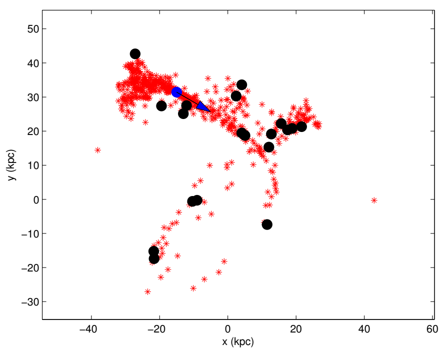

(b) The dark objects from Figure (a) with their velocity vectors. See also the color index in Figure 10.

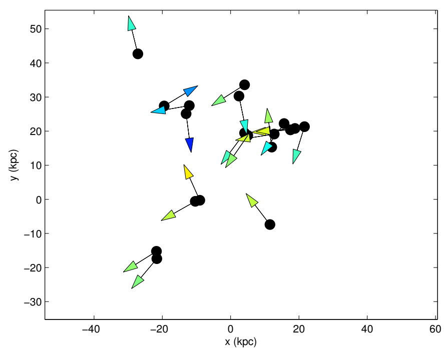

Figure 10: Color index for the velocity vectors of Figures 8b and 9b

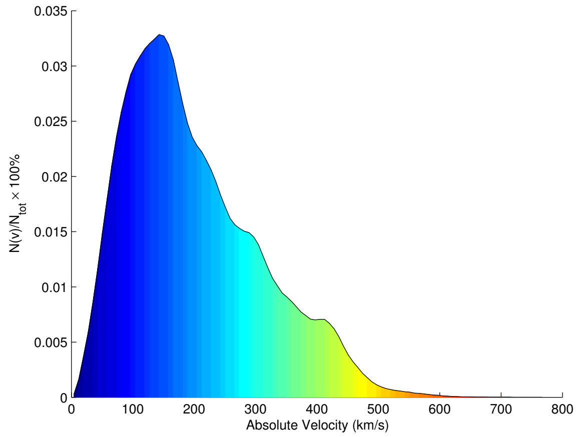

4.2 Measuring the effect of encounters

4.2.1 Potential

When Yoon et al. let their Pal-5-like stream collide with a set of dark matter objects, they noticed slanted gaps in the energy distribution (Figure 12). To check if such gaps are also present in our stream, the energy for each particle in the stream has to be calculated. The total energy of each stellar particle per unit mass is

$$E = E_{pot} + E_{kin} \tag{6}$$

where

$$E_{pot} = \Phi(r) \tag{7}$$

and

$$E_{kin} = \frac{v^2}{2} \tag{8}$$

To calculate E_{pot}, an NFW potential will be assumed:

$$\Phi(r) = \frac{-v_{vir}^2}{g(c)\frac{r}{R_{vir}}} \ln\left(1 + c\frac{r}{R_{vir}}\right) \tag{9}$$

with

$$g(x) = \ln(1+x) - \frac{1}{1+x} \tag{10}$$

Here, v_{vir} is the virial velocity, R_{vir} the virial radius and c the concentration parameter. For the virial velocity and radius, we will use the values as measured in the Aq-A-4 halo at the present day[4]:

$$R_{vir} = 245.70\,\text{kpc},\ v_{vir} = 179.37\,\text{km/s}$$

Equation (9) represents is a spherical potential, that is often used to describe dark halos formed in cold dark matter cosmological simulations. However, dark matter halos are more generally triaxial (Vera-Ciro 2011, [10]) and therefore a triaxial potential $\Phi(x, y, z)$ will be more accurate. Volgelsberger et al. [11] proposed to replace the radial distance r in Equation 9 by

$$\tilde{r} = \frac{r_E(r_a + r)}{r_a + r_E} \tag{11}$$

where

$$r_E = \sqrt{\left(\frac{x}{a_x}\right)^2 + \left(\frac{y}{a_y}\right)^2 + \left(\frac{z}{a_z}\right)^2} \tag{12}$$

[4]These values were readily available and are very close to those of the Aq-A-2 halo.

Figure 11: Number of collisions with any star for $b = 1, 2, 5\&10$kpc.

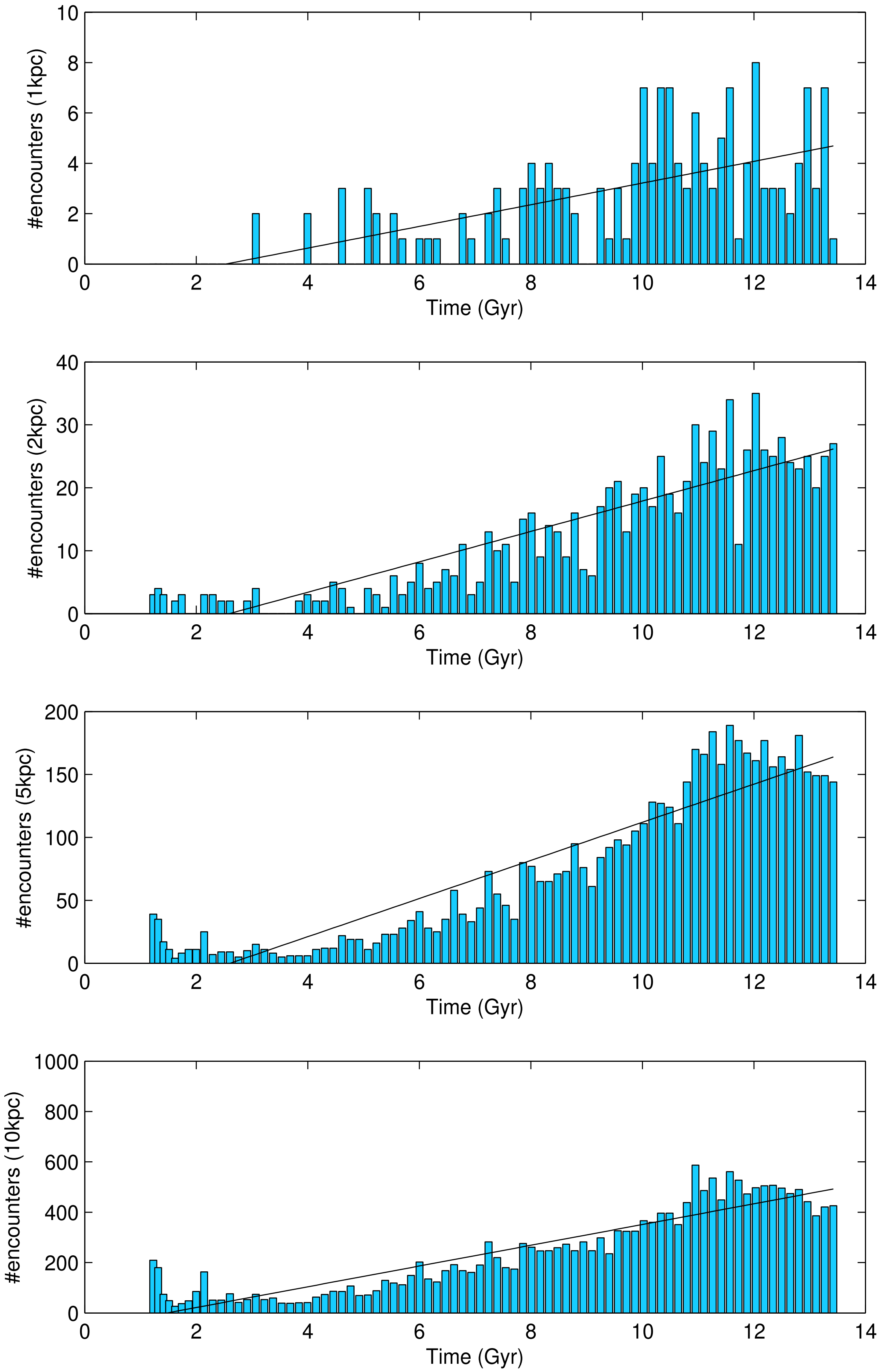

Figure 12: One of the results by Yoon et al., directly taken from [6], showing the gaps in both the spatial and energy distributions. The top/middle/bottom rows show the results in the cases that respectively the impact velocity/impact parameter (b)/subhalo mass is varied. The rightmost column shows the slanted gaps, caused by the energy shifts as predicted by Equation 19.

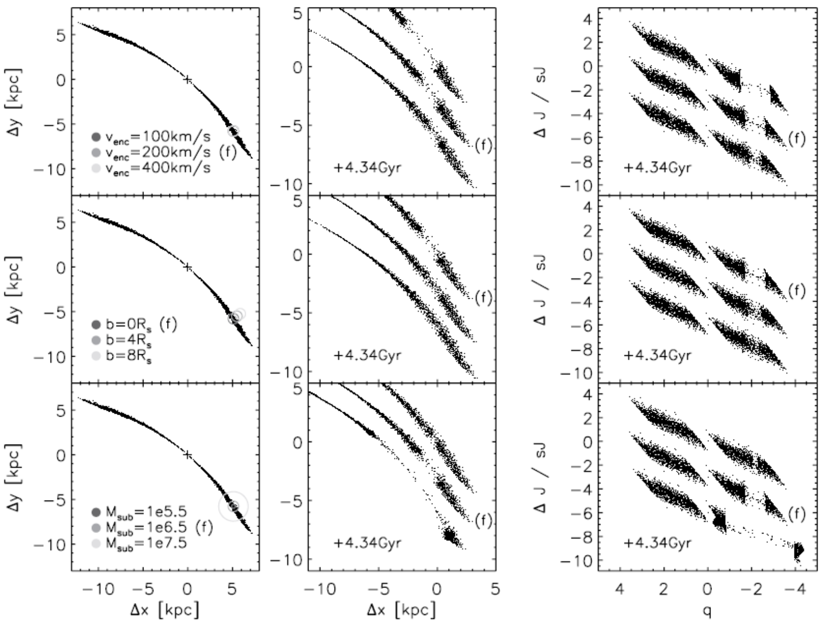

is the more general elliptical radius where the axis lengths (a_x, a_y, a_z) must be normalized so that $a_x^2 + a_y^2 + a_z^2 = 3$. r_a is the transition radius, i.e. the radius at which the potential becomes almost spherical, which is calculated from

$$r_a = k\frac{R_{vir}}{c} \tag{13}$$

We fitted the set of unknown parameters (c, k, a_x, a_y) for the Aq-A-4 main-halo at $z = 0$. Despite the lower resolution, use of these data is justified because Springel et al. [1] showed that there is good convergence between the different resolutions. The resulting values are

$$c = 16.21,\ k = 3.6,\ a_x = 1.18,\ a_y = 0.94\ \ (a_z = 0.85)$$

4.2.2 Frame of Reference

Next, we will define a spatial coordinate along the stream. A convenient coordinate would be the angle between the center of mass of the satellite and the star whose energy is measured. Thus, for each snapshot, a new coordinate system S_{stream} will be defined that meets the following criteria (Figure 13):

- The main Aquarius halo center is at the origin.
- The satellite center (i.e. the most-bound particle) lies on the positive y-axis ($x_c = 0$).
- The satellite's center velocity vector lies in the xy-plane ($v_z^c = 0$).

The unit vectors $(\hat{x}_s, \hat{y}_s, \hat{z}_s)$ for any particular snapshot i are given by

$$\hat{\mathbf{y}}_\mathbf{s}^\mathbf{i} = \frac{\mathbf{r}_c^i}{|\mathbf{r}_c^i|} \tag{14a}$$

$$\hat{\mathbf{z}}_\mathbf{s}^\mathbf{i} = \frac{\mathbf{v}_c^i \times \mathbf{r}_c^i}{|\mathbf{v}_c^i \times \mathbf{r}_c^i|} \tag{14b}$$

Figure 13: The stream system S_{stream} in which the stream lies approximately in the xy-plane, directly above main Aq-A-2 halo center. The angle θ denotes the angular distance along the stream with respect to its center.

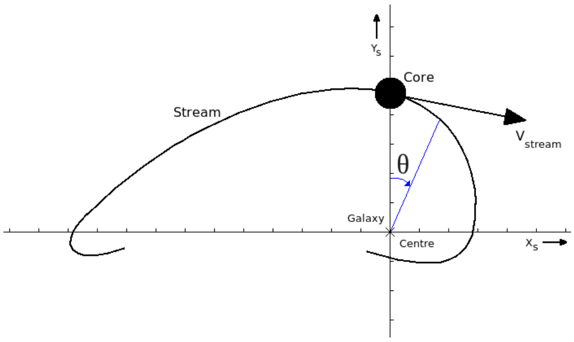

$$\mathbf{\hat{x}_s^i} = \hat{y}_s^i \times \hat{z}_s^i \tag{14c}$$

which allow for a change of coordinates to the new system (while dropping the index i for readability) $\mathbf{r} = (x, y, z) \rightarrow \mathbf{r}_s = (x_s, y_s, z_s)$:

$$(x_s, y_s, z_s) = \mathbf{r} \cdot (\hat{x}_s, \hat{y}_s, \hat{z}_s) \tag{15}$$

and

$$\theta = \arctan\left(\frac{x_s}{y_s}\right) \tag{16}$$

We also measure the z-component of the angular momentum L_z and the radial velocity v_r of each particle:

$$\frac{L_z}{M_*} = (\mathbf{r} \times \mathbf{v})_z = xv_y - yv_x \tag{17}$$

$$V_r = \frac{\mathbf{r} \cdot \mathbf{v}}{|\mathbf{r}|} \tag{18}$$

The results for $t = 4, 8, 10, 12, 14$ Gyr are plotted in Figures 14b-14f.

4.2.3 Results

Yoon et al. showed in their idealized numerical simulations that slanted gaps tend to form in the energy and spatial distribution of the stream as a result of collisions with dark subhalos, as can be seen from Figure 12. Similar features can to some extent be found in these plots as well. There are some density irregularities along the stream that could be due to the close encounters the stream experienced along its lifetime. However, since the number of particles is much smaller than in the simulations done by Yoon et al., these gaps and the expected slanting appearance are less evident.

One particularly interesting case is shown in the topleft panel of Figure 14d. As Yoon et al. showed, the energy difference during a direct encounter ($b = 0$) along the stream can be expressed as

$$\Delta E(b = 0) = 2\frac{GM_{sub}}{x}\frac{v_{stream}}{v_{enc}} \tag{19}$$

Here, x is the absolute distance measured along the stream relative to point of impact[5]. The abrupt sign-change around the impact coordinate means that particles trailing behind the point of impact will be pushed into lower energy orbits and particles preceding this point will be pushed to higher energies. This effect amplifies the already present energy gradient along the stream, causing the gaps to occur. Figure 14 depicts this energy change (Equation 19) for several subhalo masses and impact parameters. This figure shows a similarity to the small peak observed in Figure 14d which suggests that this feature might be the result of one of the collisions happening at that time and plotted in Figure 9.

[5]The spatial coordinate used in Figures 14 is the radial distance, as opposed to the absolute distance. This should however yield equivalent features.

Figure 14: The energy, angular momentum and radial velocity measured as a function of θ (Figure 13) at different moments during its evolution (a). The top left panel of each figure shows the stream in S_{stream} where also θ was measured for each particle. The top right panel shows the stream in energy/angular-momentum space and the bottom left and bottom right panels show the corresponding energy, angular momentum (z-component) and radial velocity respectively.

(a) Spatial distribution of the stream in S_{stream} (Figure 13) at different moments in time. The energy, angular momentum and radial velocity distributions are plotted in the figures below.

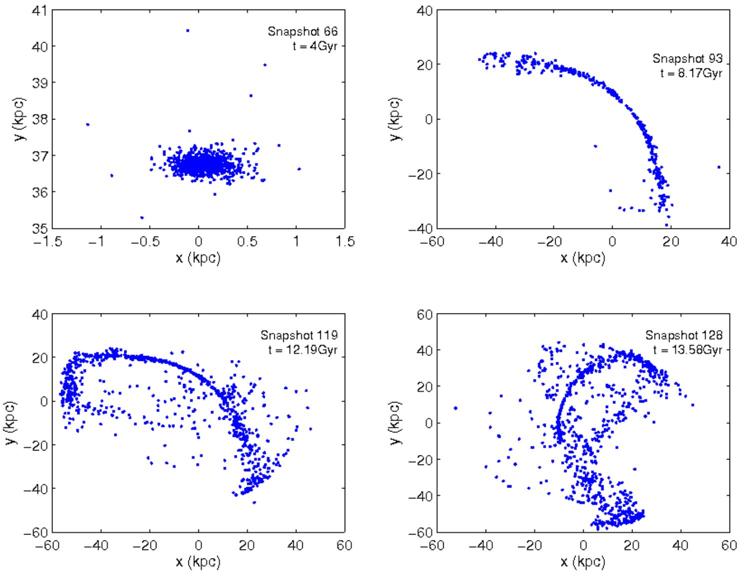

(b) The energy, angular momentum and radial velocity at $t = 4.0$ Gyr (snapshot 66).

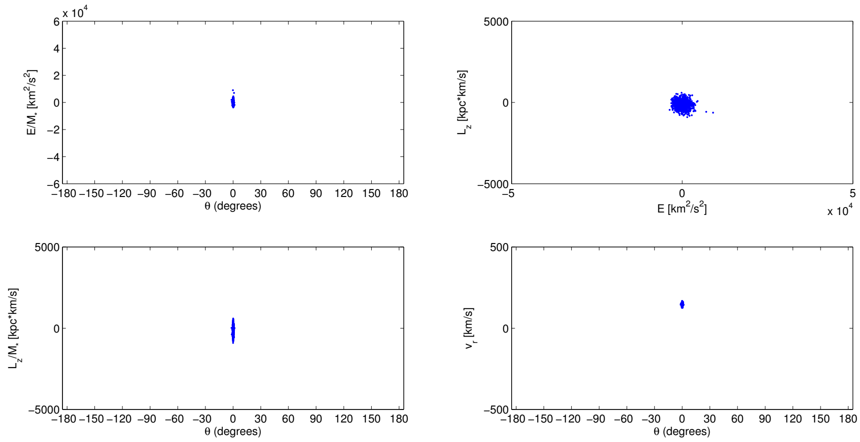

(c) The energy, angular momentum and radial velocity at $t = 8.2$ Gyr (snapshot 93).

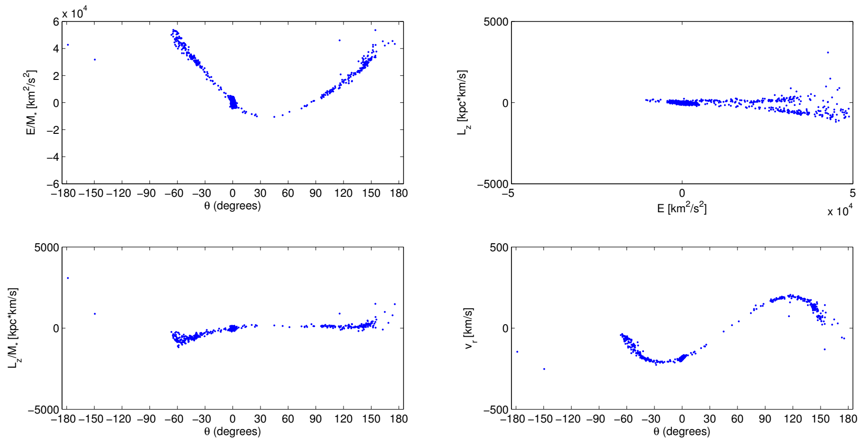

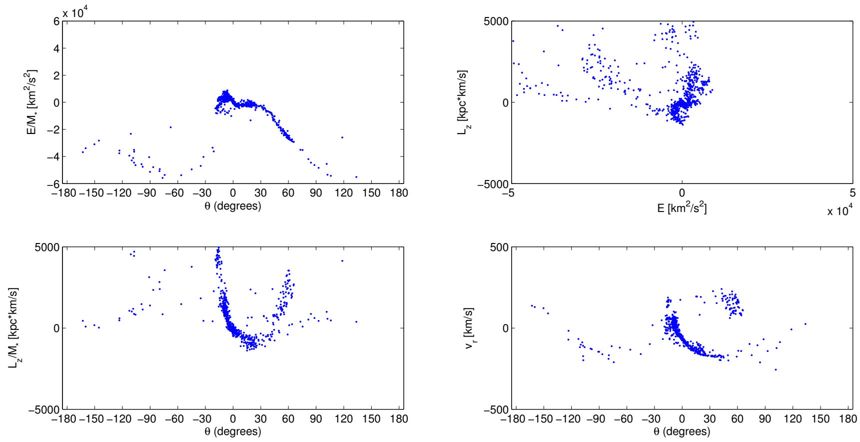

(d) The energy, angular momentum and radial velocity at $t = 10.0$ Gyr (snapshot 105).

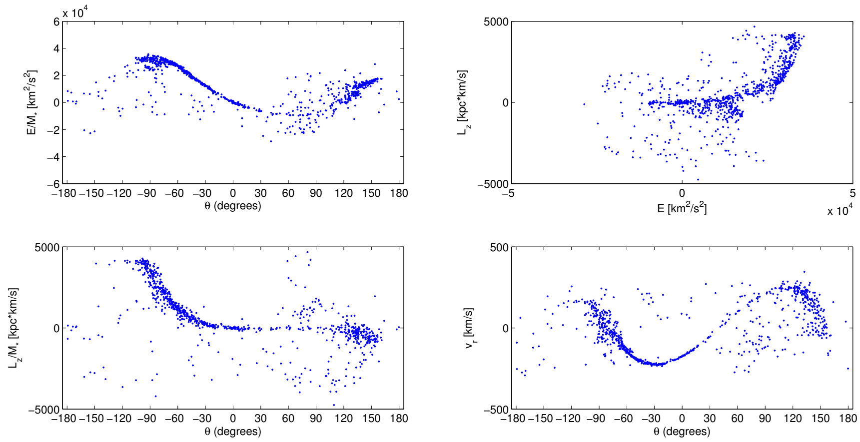

(e) The energy, angular momentum and radial velocity at $t = 12.2$ Gyr (snapshot 119).

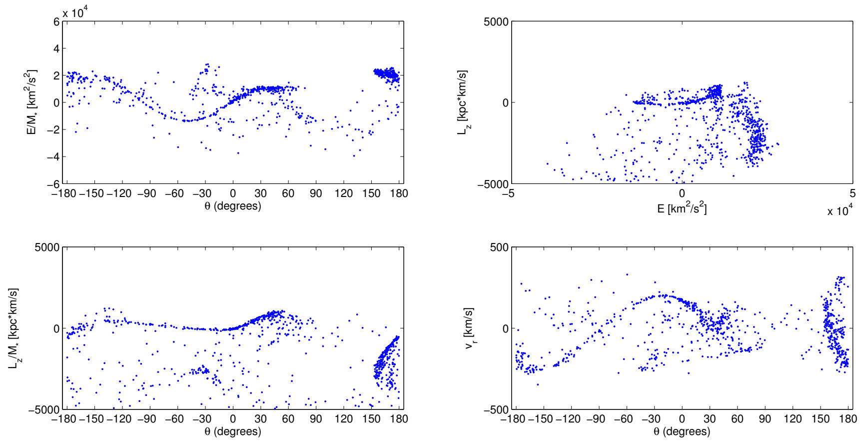

(f) The energy, angular momentum and radial velocity at $t = 13.6$ Gyr (snapshot 128).

5 Discussion

In this section we will discuss the simulations and results of previously mentioned authors ([4], [5], [6]) in a little more detail and compare them to our own results. Below we give an overview of the different simulations and their findings.

Authors	**Simulation**	**Results**
Johnston et al. (2002)	(1) $N_{halo} = 10^7$ smooth halo particles distributed as a Hernquist model (spherical time-independent potential). (2) $N_{test} = 4000$ massless test particles on perfectly circular orbits at $r = 0.5, 1.0$ kpc, evenly distributed along the entire orbit (2π), representing the streams. (3) $N_{lump} = 0$, 1, 4, 16, 64, 128, 256 lumps.	(1) Precession of the orbital plane over time in the simulations containing a larger number of lumps. (2) Smoothly distributed particles eventually become bunched together in both angular position and velocity, leaving less populated regions or gaps. (3) Large deviations (in the order of 10-50 km/s) in the radial velocity v_r from that expected in a smooth potential.
Ibata et al. (2002)	(1) Smooth, fixed potential including various Galactic components, and a halo of flattening q_m. (2) Streams initiated as a globular cluster, populated by 10^4 particles. (3) $N_{lump} = 435$, substructure modelled as softened point-mass potentials. These underestimate the forces compared to an NFW potential and therefore the scattering effiency will be reduced.	(1) Disrupted globular clusters should be substantially disrupted over the sky, even for a spherical potential ($q_m = 1$). (2) Large dispersion in the z-component of the angular momentum L_z, which should have been conserved otherwise.
Yoon et al. (2011)	(1) Smooth, spherical and time-independent NFW potential containing a varying number of subhalos. (2) A stream resembling Pal 5, represented by a 10,000 particle Plummer model of mass $10^4 M_\odot$.	(1) Streams will typically encounter multiple subhalos during their evolution. (2) Gaps will form in both the energy distribution as well as in the spatial distribution of the stream as a result of these encounters. The gaps in energy/angular-momentum-space have a slanted appearance.

The Aquarius suite does not suffer from any of the simplifications of the simulations described above, such as the assumption of e.g. a spherical potential or a time-independent mass distribution, and therefore the particles of our Orphan stream are subject to all possible effects within the host halo. Because of the resulting triaxial and time-independent potential and the non-conservation of angular momentum, the energy/angular momentum-distribution is less coherent and the evidence of multiple strong encounters in the form of gaps as seen by Yoon et al. is not as clear as it was in idealized conditions. However, we do find significant overdensities (and underdensities) in almost all distributions (both spatial and energetic). This result cannot solely be accounted for by the triaxial shape of the potential.

Because of the low time-resolution, it is very probable that several collisions have gone un-

Figure 14: These plots are directly taken from Yoon et al. [6] and display the shifts in energy (Equation 19) as a function of the position along the stream with respect to the point of impact. The left panel shows the effect of different subhalo masses: $5 \times 10^5 - 5 \times 10^9\ M_{\odot}$. The right panel shows the result for a subhalo of mass $5 \times 10^7\ M_{\odot}$ passing by at $b = 0, 2, 4, 8, 16$ kpc. The energy scale is normalized by a characteristic energy, which is defined as $\Delta E_{char} = \Delta E(b = 0;\ x = r_s;\ v_{stream} = v_{stream}^{typ};\ v_{enc} = v_{enc}^{typ})$.

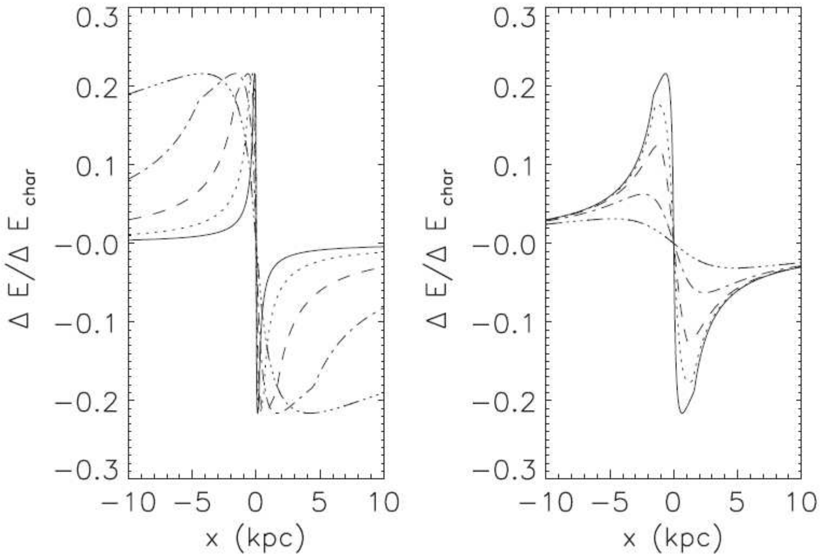

detected. Also, since the number of stars that belong to our Orphan stream is quite low (857), compared to the work described above, the overdensities are less clear than they would have been if more particles were involved.

In future work, it would be desirable to use the outputs with a higher sampling in time[6]. Another interesting aspect would be to establish the effects of the different masses of the impacting subhalos onto the stream and how they are related to the gaps. Nonetheless, we can conclude that it is highly unlikely for a stream not to have encountered multiple (heavy) subhalos during its evolution. If the missing satellites do exist, each luminous satellite will have encountered them on multiple occasions and the fingerprints of these encounters should still be visible, even in complex N-body cosmological simulations or the real world.

[6]Originally, 1024 outputs for the Aq-A-2 have been stored.

References

[1] Springel et al., 2008, MNRAS, 391, 1685

[2] Klypin A., Kravtsov A. V., Valenzuela O., Prada F., 1999, ApJ, 522, 82

[3] Helmi A., Cooper A. P., White S. D. M., Cole S., Frenk C. S., Navarro J. F., 2011, ApJ, 733, L7

[4] Johnston K. V., Spergel D. N., Haydn C., 2002, ApJ, 570, 656

[5] Ibata R. A., Lewis G. F., Irwin M. J., Quinn T., 2002, MNRAS, 332, 915

[6] Yoon J. H., Johnston K. V., Hogg D. W., 2011, ApJ, 731, 58

[7] Cooper et al., 2010, MNRAS, 406, 744

[8] Belokurov et al., 2007, ApJ, 658, 337

[9] Sparke L, Gallagher J, 2000, *Galaxies in the Universe*, Cambridge University Press, Cambridge, p. 125

[10] Vera-Ciro et al., 2011, MNRAS, 416, 1377

[11] Vogelsberger M., White S. D. M., Helmi A., Springel V., 2008, MNRAS, 385, 236

[12] Ibata R., Lewis G. F., Irwin M., Totten E., Quinn T., 2000, ApJ, 551, 294